Chinese Chemical Letters 37 (2026) 111299

Contents lists available at ScienceDirect

Chinese Chemical Letters

journal homepage: www.elsevier.com/locate/cclet

Microwave-sensitive Al-based nano-immunoadjuvant for strengthened tumor microwave-immunotherapy *via* programmed activation of NLRP3-mediated pyroptosis

Zengzhen Chen[a,1], Lirong Zhao[a,c,1], Wenna Guo[a,b], Longfei Tan[a], Qiong Wu[a], Changhui Fu[a], Xiangling Ren[a], Shiping Yu[d,*], Xiaowei Chen[f,*], Nam-Young Kim[e], Guihua Jiang[b], Xianwei Meng[a,*]

[a] *State Key Laboratory of Cryogenic Science and Technology, Technical Institute of Physics and Chemistry, Laboratory of Controllable Preparation and Application of Nanoparticles, Chinese Academy of Sciences, Beijing 100190, China*
[b] *The Department of Medical Imaging, The Affiliated Guangdong Second Provincial General Hospital of Jinan University, Guangzhou 518037, China*
[c] *Shanxi Pharmaceutical Vocational College, Taiyuan 030031, China*
[d] *Department of Interventional Therapy, Shanxi Province Cancer Hospital, Shanxi Hospital Affiliated to Cancer Hospital, Chinese Academy of Medical Sciences, Cancer Hospital Affiliated to Shanxi Medical University, Taiyuan 030000, China*
[e] *RF Bio Center, Department of Electronic Engineering, Kwangwoon University, 20 Kwangwoon-ro, Nowon-gu, Seoul 01897, South Korea*
[f] *Department of Interventional Radiology, First Hospital of China Medical University, Shenyang 110001, China*

ARTICLE INFO

Article history:
Received 31 December 2024
Revised 1 May 2025
Accepted 9 May 2025
Available online 10 May 2025

Keywords:
Microwave thermal therapy
Immunosuppressive
NLRP3
Pyroptosis
αPD-L1 therapy

ABSTRACT

Immunosuppressive tumor microenvironment (TME) is a key regulator in the high recurrence and metastasis rate of breast cancer after microwave (MW) thermal therapy. Pyroptosis, a form of programmed cell death initiated by inflammasomes, which can activate tumor immunogenicity and reprogram immune TME. Here, we report an extremely simple Al-based metal-organic frameworks nano-immunoadjuvants (AM NIAs) that programmatically activate nucleotide-binding domain, leucine-rich-containing family, pyrin domain-containing-3 (NLRP3)-mediated pyroptosis to enhance MW-immunotherapy (MW-ICB). After entering the TME, AM NIAs programmed activation of NLRP3-mediated pyroptosis by inducing mitochondrial dysfunction, upregulating HSP90 and promoting lysosomal stress. Consequently, substantial amounts of lactate dehydrogenase, interleukin-18 (IL-18), and calreticulin are released, which improves immunosuppressive TME and hinders tumor cell proliferation by facilitating T-cell infiltration. The integration of immune checkpoint inhibitors with MW elicits potent immune responses, demonstrating high inhibition of both primary and distant tumors. Thus, a simple yet effective nano-immunoadjuvant is developed to enhance MW-ICB in breast cancer simply by NLRP3-mediated pyroptosis and immunosuppression reversal.

© 2025 Published by Elsevier B.V. on behalf of Chinese Chemical Society and Institute of Materia Medica, Chinese Academy of Medical Sciences.

Breast cancer has become one of the most prevalent malignancies in women, with the highest mortality rate among female cancer-related deaths [1]. Microwave (MW) thermal therapy is a minimally invasive technique with several advantages of reduced invasiveness, abbreviated treatment duration, deep tissue penetration, and minimal adverse effects, which has become the preferred treatment option for breast cancer patients who are resistant to radiotherapy/chemotherapy, in poor physical condition or inoperable [2–5]. However, larger or irregularly shaped tumors are prone to sublethal thermal stress during MW thermal therapy, leading to residual tumor [6,7]. This residual tumor often results in recurrence and metastasis, significantly threatening patient survival and hindering the widespread clinical application of MW thermal therapy [8–10].

Immunotherapy, including immune checkpoint blockade (ICB) therapy, has demonstrated promising clinical potential in preventing tumor recurrence and metastasis by effectively activating the patient's own immune system to elicit a sustained and potent antitumor response [11–13]. Consequently, the integration of immune checkpoint inhibitors (ICIs) with MW thermal therapy holds promise as an effective anticancer strategy. Nevertheless, the weak

* Corresponding authors.
E-mail addresses: yushiping6@126.com (S. Yu), cxwcmu@163.com (X. Chen), mengxw@mail.ipc.ac.cn (X. Meng).
[1] These authors contributed equally to this work.

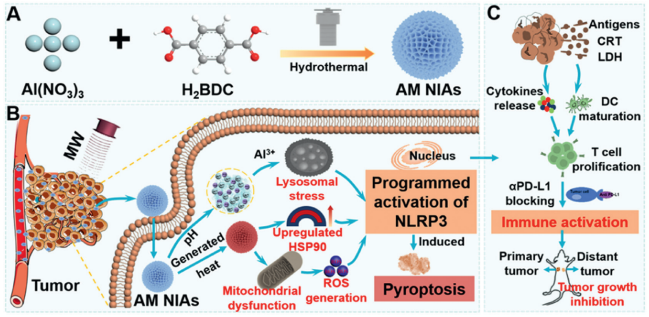
https://doi.org/10.1016/j.cclet.2025.111299
1001-8417/© 2025 Published by Elsevier B.V. on behalf of Chinese Chemical Society and Institute of Materia Medica, Chinese Academy of Medical Sciences.

immune response elicited by thermal therapy and the complex immunosuppressive tumor microenvironment (TME) impede the efficacy of ICIs in enhancing immune responses, potentially rendering the treatment ineffective [14–16]. Therefore, it is imperative to investigate novel strategies capable of augmenting antitumor immune responses and reprogramming the immunosuppressive TME to mitigate the risk of tumor recurrence in MW-ICB therapy for breast cancer.

Precisely modulating tumor cell inflammatory death, such as cuproptosis, ferroptosis, necroptosis, and pyroptosis [17–20], has emerged as a promising strategy for remodeling the immunosuppressive TME and augmenting the immunotherapy response. Pyroptosis is a recently identified type of programmed cell death characterized by cellular swelling, membrane rupture, DNA fragmentation, and the release of pro-inflammatory cytokines, which is triggered by inflammatory caspase-mediated gasdermin cleavage [21,22]. The pro-inflammatory cytokines (*e.g.*, interleukin (IL)-18) and damage-associated molecular patterns (DAMPs) released during pyroptosis can elicit a strong inflammatory response [23,24], conferring high immunogenicity to the tumor and resulting in an effective antitumor immune response [25,26], such as enhanced tumor phagocytosis by tumor-associated macrophages and increased function and number of $CD8^+$ T cells [27,28]. Thus, pyroptosis represents a novel approach to effectively enhance antitumor immune responses, providing a new strategy to reduce tumor recurrence and improve the efficacy of breast cancer therapy.

Nucleotide-binding domain, leucine-rich-containing family, pyrin domain-containing-3 (NLRP3) proteins are key regulators of pyroptosis, which restricts the occurrence of cell pyroptosis [29,30]. Activating and regulating NLRP3 expression can induce pyroptosis in tumor cells. Current efforts focus on developing bioactive materials containing specific metal ions to activate NLRP3-mediated pyroptosis [31,32]. For example, Cheng *et al.* developed bioactive zinc-nickel hydroxide ($ZnNi(OH)_4$) nanosheets, which can effectively initiate a positive feedback cycle of pyroptosis through a synergistic ionic effect to enhance the efficacy of immunotherapy [23]. Despite encouraging advances in metal ion-induced cellular pyroptosis to enhance immunotherapeutic efficacy, while metal ion-induced pyroptosis lacks specificity, and systemic administration of metal ions may cause uncontrolled pyroptosis in normal cells [33,34]. Additionally, therapeutic strategies involving the use of cytotoxic reactive oxygen species (ROS) to activate NLRP3 face the challenge of efficient ROS production [35,36]. Furthermore, there were few reports on microwave-enhanced pyroptosis biomaterials in activating the NLRP3 pathway to induce pyroptosis in tumor cells. Therefore, the development of nano-immunoadjuvants tailored to the post-MW thermal therapy TME, which possess both MW sensitization and activation of NLRP3-mediated pyroptosis properties is essential to enhance the synergistic antitumor effects of MW-ICB for breast cancer.

As a proof of concept, we demonstrated an extremely simple MW-immunosensitizing Al-based metal-organic frameworks nano-immunoadjuvants (AM NIAs) that programmatically activate NLRP3-mediated cell pyroptosis to elicit a potent antitumor immune response for enhanced MW-ICB treatment of breast cancer (Scheme 1). Upon intravenous administration, AM NIAs were efficiently internalized by tumor cells. Subsequently, AM NIAs programmed to activate NLRP3-induced cell pyroptosis proceeds through the following mechanisms: (1) MW thermal therapy causes mitochondrial damage, leading to increased ROS production, which activates the NLRP3 inflammasomes and enhances the secretion of inflammatory cytokines, ultimately inducing pyroptosis; (2) heat shock protein 90 (HSP90) acts as a stabilizing and activating factor for NLRP3. MW thermal therapy induces acute heat stress, upregulating HSP90 expression to bolster cellular heat stress resistance and activate the HSP90-NLRP3 pathway; (3) AM NIAs



Scheme 1. Schematic representation of the synthesis of MW-sensitive AM NIAs and its enhancement of MW-ICB through programmed activation of NLRP3-mediated pyroptosis. (A) The synthesis of AM NIAs. (B) Mechanism of programmed activation of NLRP3-mediated cell pyroptosis by AM NIAs combined with MW. (C) Mechanism of AM NIAs-triggered pyroptosis combined with αPD-L1 strategy to elicit a potent antitumor immune response that effectively suppresses primary and distant tumors.

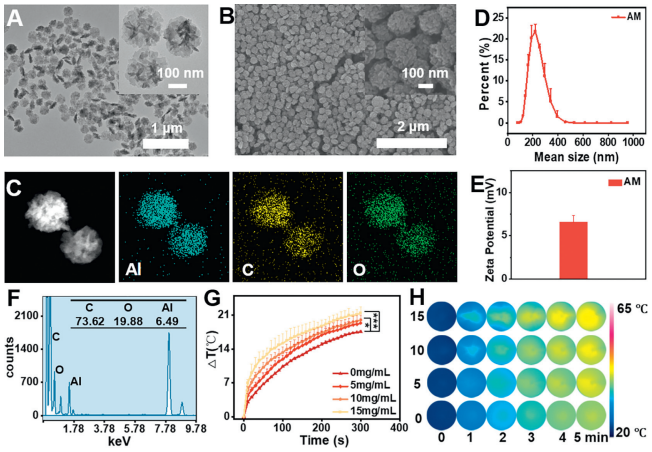


Fig. 1. Fabrication and characterization of AM NIAs. (A, B) The TEM and SEM image of AM NIAs. (C) The TEM-Mapping (C, O, and Al) of AM NIAs. (D-H) The dynamic light scattering and zeta-potential value, EDS analysis, temperature rose curve and thermal infrared diagram of AM NIAs ($n = 3$). Data are presented as mean ± standard deviation (SD). $^*P < 0.05$, $^{***}P < 0.001$.

release highly reactive Al^{3+} ions upon structural disintegration in the acidic TME. The interaction of aluminum-containing adjuvants with lysosomes induces lysosomal stress, activating the NLRP3 inflammasomes and triggering intense pro-inflammatory cell death, thus activating antitumor immunity. Importantly, this novel therapeutic strategy induced the release of IL-18 and calreticulin (CRT), which promoted T cell infiltration and significantly inhibited tumor cell proliferation, achieving a tumor suppression rate of 96.50 %. Furthermore, when combined with ICB therapy, this innovative approach elicited a robust systemic immune response, effectively suppressing both primary and distant tumors. Collectively, these findings suggested that AM NIAs can serve as an innovative and efficient platform for MW-enhanced pyroptosis, facilitating the integration of MW thermal therapy with immunotherapy to achieve systemic antitumor therapeutic effects initiated by local MW thermal treatment.

In this work, we have prepared AM NIAs by a simple one-step hydrothermal synthesis using Al^{3+} as the central metal ion and 1,4-dicarboxybenzene as the organic ligand. Subsequently, we observed the morphological features of AM NIAs by scanning electron microscopy (SEM) and transmission electron microscopy (TEM). As shown in Figs. 1A and B, AM NIAs presented a regular spherical nanoflower structure with good dispersion. TEM-mapping and energy dispersive X-ray spectra (EDS) results demonstrated the pres-

ence and distribution of the elements C (73.62 %), O (19.88 %) and Al (6.49 %) in AM NIAs (Figs. 1C and F). Afterwards, the particle size and potential of AM NIAs were measured by Malvern Zetasizer nano-ZSE, which showed an average hydrated diameter of 220.2 nm and a zeta-potential of 6.59 ± 0.73 mV (Figs. 1D and E). Furthermore, the X-ray diffraction spectra of AM NIA showed many peaks, especially sharp peaks at 5.01°, 9.11°, 15.27°, and 17.59° (Fig. S1 in Supporting information). Taken together, these results validate the successful synthesis of AM NIAs.

After that, we investigated the MW thermal sensitization performance of AM NIAs. As shown in Fig. 1G, we found that under MW irradiation (5 min, 0.6 W/cm^2), the temperatures of AM NIAs (0, 5, 10, and 15 mg/mL) solutions with different mass concentrations increased to 17.6, 19.4, 20, and 21.47 °C, respectively, indicating that AM NIAs had good MW thermal sensitization, which was more visualized by the results of forward-looking infrared imaging (Fig. 1H). Therefore, AM is expected to act as a pyroptosis nanoimmunoadjuvant to improve the efficacy of tumor MW thermal therapy.

Next, we assessed the biosafety of AM NIAs. Firstly, we examined the cytotoxicity of AM NIAs by methyl thiazolyl tetrazolium (MTT) solution. As shown in Fig. 2A, AM NIAs still showed excellent biosafety with 82.59 % cell viability at mass concentrations up to 1000 μg/mL. Then, we tested the acute toxicity of AM NIAs *in vivo*. The results demonstrated that when the concentration of AM NIAs reached 100 mg/kg, the mice displayed no significant abnormalities in body weight changes (Fig. 2B), blood routine examination (Fig. 2C), and major tissue hematoxylin-eosin (H&E) staining analysis (Fig. S2 in Supporting information). Moreover, the hemocompatibility of AM NIAs was further assessed by hemolysis assay. The supernatants were essentially transparent and colorless,

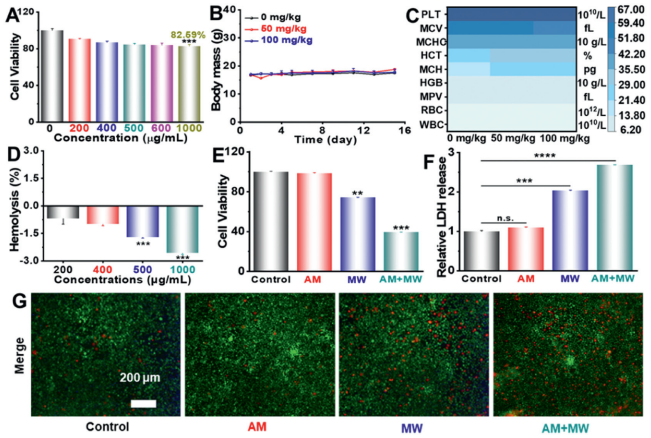


Fig. 2. Biosafety and cell inhibition of AM NIAs. (A) Viability of 4T1 cells under incubation with different mass concentrations of AM NIAs ($n = 5$). (B, C) Changes in body weight and routine blood tests of mice in each group after injection of different mass concentrations of AM NIAs ($n = 3$). (D) Hemolytic test results of AM NIAs ($n = 3$). (E) Viability of 4T1 cells under different treatments ($n = 5$). (F) Relative amount of LDH released by different treatment ($n = 5$). (G) Fluorescence images of 4T1 cells in different treatment groups co-stained with calcein-AM and PI. Data are presented as mean ± SD. $^{**}P < 0.01$, $^{***}P < 0.001$, $^{****}P < 0.0001$.

at mass concentrations of 0, 200, 400, 500, and 1000 μg/mL, respectively (Fig. 2D and Fig. S3 in Supporting information). Hemolysis rate of AM NIAs was detected by ultraviolet-visible (UV–vis) spectroscopy as 0.69 %, 1.00 %, 1.71 % and 2.58 %, respectively, which showed outstanding hemocompatibility.

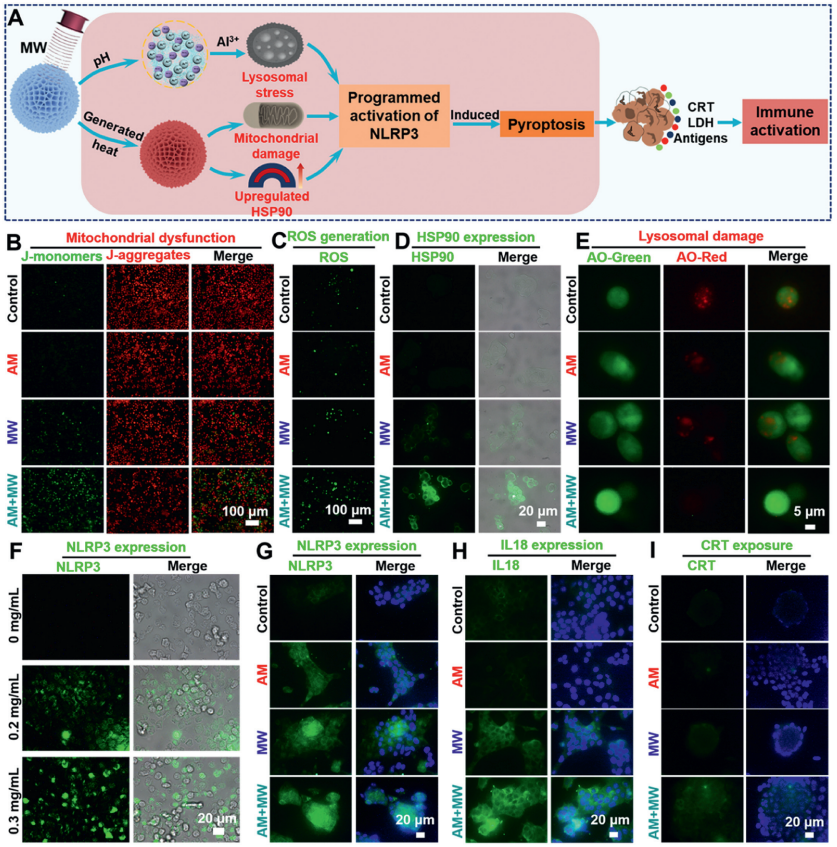


Fig. 3. AM NIAs trigger NLRP3 to induce pyroptosis and enhance antitumor immunity. (A) Schematic diagram of AM NIAs triggering NLRP3 to induce apoptosis and enhance anti-tumor immunity. (B-E) Fluorescence images of $\Delta\psi_m$, ROS production, HSP90 expression, and lysosomal stress. (F) Fluorescence results of NLRP3 expression after 24 h incubation with different mass concentrations of AM NIAs. (G-I) Fluorescence results of NLRP3 expression, IL-18 expression, and CRT exposure under different treatments.

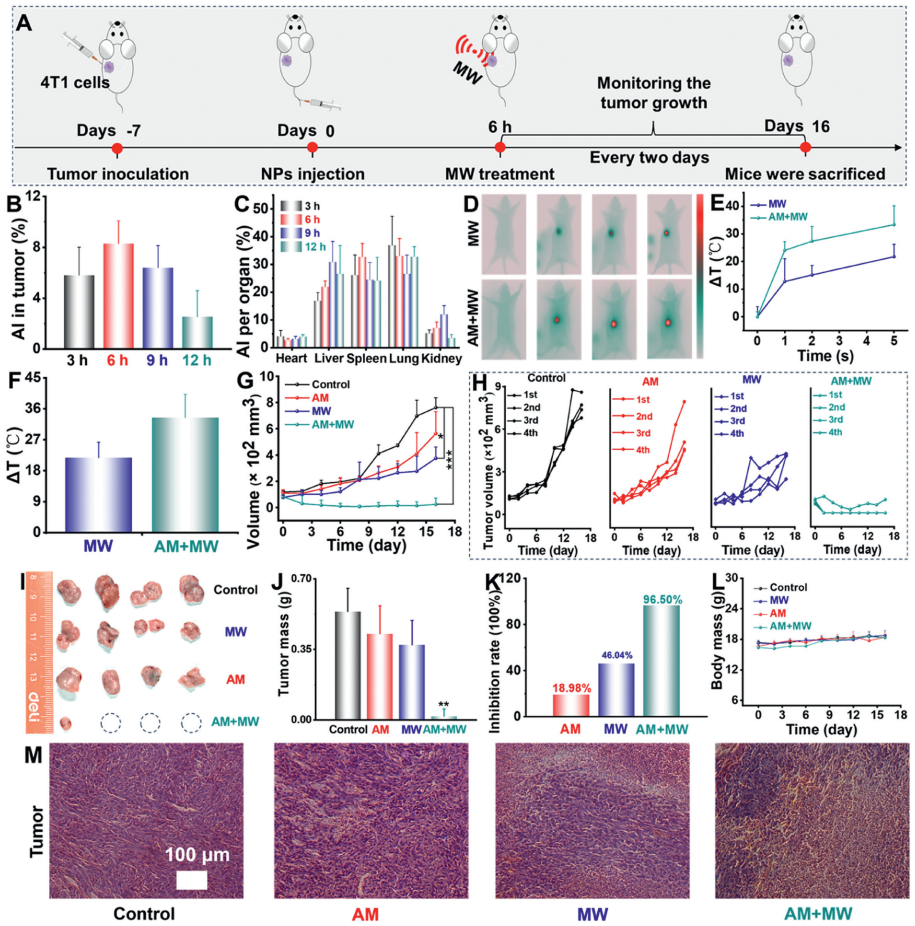


Fig. 4. Evaluation of AM NIAs-induced cell pyroptosis to enhance antitumor efficacy *in vivo*. (A) Schematic diagram of MW thermal therapy and monitoring in mice ($n = 4$). (B, C) Distribution of Al^{3+} in tumor, heart, liver, spleen, lungs and kidneys at 3, 6, 9 and 12 h of injection ($n = 3$). (D–F) The results of thermal imaging image, temperature change curves and final temperature indifferent groups of tumors under MW irradiation. (G–K) The tumor volume curves, tumor growth curves, tumor tissues, tumor mass, and tumor inhibition rates in different groups ($n = 4$). (L, M) Body weight change curves and H&E staining results of tumor tissues within 16 days after different treatment ($n = 4$). Scale bar: 100 μm. Data are presented as mean ± SD. $^{*}P < 0.05$, $^{**}P < 0.01$, $^{***}P < 0.001$.

Afterwards, we investigated the inhibitory effect of AM NIAs *in vitro*. As shown in Fig. 2E, the cell viability was similar in the AM NIAs alone group and the control group, which confirmed its good biosafety. After introducing MW, the cell viability of the MW group decreased to 74.25 %. While the AM NIAs + MW group had the lowest cell viability of only 39.42 %, which had the best tumor therapeutic effect. Subsequently, we further analyzed the tumor cell viability of different treatment groups using calcitonin and propidium iodide (calcein-AM/PI, Fig. 2G and Fig. S4 in Supporting information). The results demonstrated that the AM NIAs + MW group had the strongest red fluorescence, indicating that its inhibitory effect on 4T1 cells was the most obvious and most of the tumor cells died. Therefore, AM NIAs-mediated MW thermal therapy can significantly kill tumor cells.

The occurrence of pyroptosis releases intracellular contents, including lactate dehydrogenase (LDH), pro-inflammatory cytokines (such as IL-18), and DAMPs. In this work, we demonstrated that AM NIAs can programmed activation of NLRP3 by several aspects such as mitochondrial dysfunction, HSP90 expression and lysosomal stress (Fig. 3A), which in turn induced tumor cells to undergo pyroptosis.

Firstly, LDH is one of the important markers of content leakage after tumor cells undergo pyroptosis. As shown in Fig. 2F, the LDH release in the MW-treated group was higher than that in the control group, while the AM NIAs + MW group showed the highest LDH release, indicating that AM NIAs could effectively induce pyroptosis in 4T1 cells. Secondly, we examined mitochondrial dysfunction caused by MW thermal therapy. As shown in Fig. 3B, JC-1 staining results displayed that AM NIAs could cause minor mitochondrial damage, and MW treatment could aggravate the damage, while AM NIAs combined with MW showed serious mitochondrial membrane potential ($\Delta\psi_m$) decline. These results demonstrated that the mitochondrial polarization induced by AM NIAs after MW treatment was conducive to the effective promotion of cell pyroptosis. Next, we assayed mitochondrial dysfunction-induced intracellular ROS production (Fig. 3C) to promote cell pyroptosis. Weak fluorescence was detected after AM treatment alone. Both MW and AM NIAs + MW treatments showed bright green fluorescence compared to controls, verifying that the introduction of MW accelerated mitochondrial dysfunction and induced more intracellular ROS production. Subsequently, we examined the expression of HSP90 in different treatment groups (Fig. 3D). The cellular immunofluorescence results confirmed that MW thermal therapy could upregulate the expression of HSP90, and the introduction of AM NIAs could further enhance its expression. Finally, we also tested the lysosomal stress response of cells in different treatment groups. As shown in Fig. 3E, the red fluorescence gradually diminished and green fluorescence was enhanced after AM NIAs treatment compared with the control group. While almost no red fluorescence was observed in the AM NIAs combined with MW, which confirmed the occurrence of lysosomal stress response. The above results indicate that AM NIAs-mediated MW thermal ther-

apy can cause mitochondrial dysfunction, upregulate HSP90 expression, and trigger lysosomal stress, which is beneficial to programmed activation of NLRP3 inflammasome to induce tumor cell pyroptosis.

Afterwards, we investigated the effect of AM NIAs combined with MW on the activation of the NLRP3 pathway. Fig. 3F showed that the green fluorescence gradually increased with increasing mass concentration of AM NIAs, which indicated that the expression of NLRP3 inflammasome increased with the increase of AM NIAs mass concentration. Correspondingly, the longer the incubation time with AM NIAs, the brighter the green fluorescence of NLRP3 inflammasome (Fig. S5 in Supporting information). In addition, the expression of NLRP3 was significantly increased under MW irradiation (Fig. 3G), suggesting that AM NIAs in combination with MW can programmed activation of NLRP3 pathway to induce tumor cell pyroptosis.

Afterwards, we investigated the expression level of IL-18 protein, one of the important markers of cell pyroptosis. The cell fluorescence results in Fig. 3H showed that AM NIAs induced the release of the inflammatory cytokines IL-18 produced by cell pyroptosis. The introduction of MW can accelerate the release of IL-18, and the AM NIAs + MW treatment group had the highest fluorescence intensity, which indicated that AM NIAs combined with MW could effectively induce the release of IL-18. Subsequently, we further verified the cellular pyroptosis-mediated immunogenic cell death (ICD) effect, and we measured the exposure of CRT. As depicted in Fig. 3I, the green fluorescence of CRT was enhanced after treatment with AM NIAs. While the green fluorescence of CRT was significantly increased under MW irradiation, suggesting that AM NIAs + MW induced 'eat-me' signals in tumor cells, which enhanced the immune response.

Based on the promising antitumor properties of AM NIAs *in vitro* under MW irradiation, we further evaluated the antitumor efficacy of AM NIAs combined with MW in 4T1 tumor-bearing mice (Fig. 4A). During animal experiments, we strictly followed the Guidelines for Assessment and Approval of Laboratory Animal Care (No. IACUC-IPC-23094) approved by the Laboratory Animal Management Committee of TIPC, CAS. Firstly, we investigated the optimal time of MW treatment of AM NIAs after injection. Fig. 4B showed the results of AM NIAs enrichment within the tumors of mice, and it can be observed that the highest concentration of enrichment was observed at 6 h (8.28 %), which suggested that the optimal time for MW treatment was 6 h after injection. Furthermore, we also investigated the biodistribution of AM NIAs in different organs. As shown in Fig. 4C, within 12 h of injection, AM NIAs was mainly concentrated in the liver, spleen, lungs, and kidneys which was responsible for removing AM NIAs.

After that, we conducted an antitumor therapy. Figs. 4D–F showed that the temperature of the tumor region increased by 21.75 °C in the MW group and 33.38 °C in the AM NIAs + MW group, further proving the accumulation of AM NIAs in the tumor tissues and its excellent MW sensitizing properties. At the end of the treatment, we measured the tumor volume and body weight of the mice every two days. The tumor volume results showed a slight delay in tumor growth in the AM NIAs group of mice compared to the control group (Figs. 4G and H). MW induced cell pyroptosis, resulting in moderate tumor growth inhibition in the MW group. Due to AM NIAs enhanced MW thermal therapy-induced cell pyroptosis and activation of immune response, the tumor inhibition was the most obvious in AM NIAs + MW group. Figs. 4I and J displayed the tumor size and mass of the mice in each treatment group, and it can be clearly observed that the AM NIAs combine with MW had the smallest tumor remnants, where even 3 mice were completely cured of their tumors. Moreover, it can be seen from Fig. 4K that the tumor inhibition rate of AM NIAs + MW group was up to 96.50 %, which further confirmed that

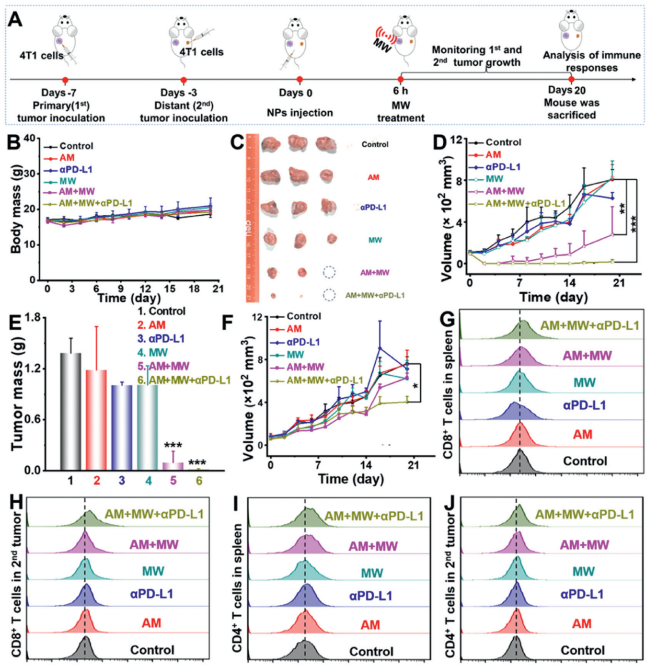


Fig. 5. Sensitization of MW-αPD-L1 immunotherapy *via* AM NIAs. (A) Schematic diagram of treatment for bilateral tumor model. (B) Body weight change curves in mice within 20 days after different treatment. (C–F) The tumor tissues, tumor volume curves, tumor mass of primary tumors, and tumor volume curves of distant tumors in different group. (G–J) Flow cytometry results of $CD8^+$ T cells and $CD4^+$ T cells in spleen and distant tumors of each group. Data are presented as mean ± SD ($n = 3$). $^*P < 0.05$, $^{**}P < 0.01$, $^{***}P < 0.001$.

AM NIAs enhanced cell pyroptosis and activated the immune response induced by MW thermal therapy to achieve a good tumor inhibition effect. No significant abnormalities were found in body weight, tissues and organs of mice in each treatment group (Fig. 4L and Fig. S6 in Supporting information), which verified the excellent biosafety of AM NIAs. Fig. 4M showed the H&E staining results of tumor tissues in each treatment group. The results showed that the tumor cells in the AM NIAs + MW group were the most severely damaged compared with the other groups, indicating that AM NIAs enhanced the antitumor effect.

Inspired by the outstanding performance of AM NIAs + MW, the *in vivo* systemic antitumor efficacy of combined anti-PD-L1 antibody (αPD-L1) therapy was investigated (Fig. 5A). Mice with bilateral 4T1 tumors were randomly divided into 6 groups, with the right tumor subjected to treatment defined as primary tumor and the left tumor remained untreated defined as distant tumor. Fig. 5B displayed that mice did not experience significant abnormalities in body weight after the various treatments, suggesting the absence of any notable side effects associated with the combination treatment. As expected, the AM NIAs + MW + αPD-L1 group had the best therapeutic efficacy against the primary tumor, indicating a significant therapeutic advantage of the combination strategy (Figs. 5C–E). Furthermore, the application of AM NIAs + MW to the treatment of primary tumors resulted in a partial reduction of distant tumor growth. And when combined with αPD-L1, it synergistically enhanced the inhibitory effect on distant tumors (Fig. 5F). Subsequently, we analyzed the expression of $CD8^+$ T and $CD4^+$ T cells in the spleens, primary tumors and distant tumors of mice by flow cytometry (Figs. 5G–J and Fig. S7 in Supporting information). The results revealed that the AM NIAs + MW + αPD-L1 group had the highest expression of both $CD8^+$ and $CD4^+$ T cell, leading to the most pronounced tumor suppression effect, which was like the tumor volume curve. Therefore, the combination of AM NIAs + MW

with ICIs holds promise for suppressing the proliferation of both primary tumors and distant tumors.

In summary, we have successfully constructed and prepared an extremely simple AM NIAs nano-immunoadjuvant that enhances MW-ICB in breast cancer by programmatically activating NLRP3-mediated pyroptosis to trigger a potent antitumor immune response. The programmed activation of NLRP3 by AM NIAs under MW irradiation involved the following mechanisms: (1) MW thermal therapy-induced mitochondrial dysfunction leading to ROS production; (2) MW thermal therapy-triggered acute heat stress upregulating HSP90 expression; (3) aluminum adjuvant interaction with lysosomes causing lysosomal stress. Subsequently, large amounts of LDH, IL-18 and CRT were released intracellularly to reprogrammed the immune TME and promote T-cell activation and infiltration for antitumor immunity. When combined with ICB, this innovative strategy elicited a strong systemic immune response and has demonstrated promising therapeutic outcomes in bilateral breast cancer models. As such, this study offers a simple and effective nano-immunoadjuvant for reversing the immunosuppressive TME in breast cancer to enhance MW-immunotherapy, which opens new avenues for effectively preventing tumor recurrence and metastasis.

Declaration of competing interest

The authors declare that they have no known competing financial interests or personal relationships that could have appeared to influence the work reported in this paper.

CRediT authorship contribution statement

Zengzhen Chen: Writing – review & editing, Funding acquisition, Conceptualization. **Lirong Zhao:** Writing – review & editing, Methodology, Investigation. **Wenna Guo:** Writing – review & editing, Methodology, Investigation. **Longfei Tan:** Writing – review & editing, Methodology, Investigation. **Qiong Wu:** Writing – review & editing, Methodology, Investigation. **Changhui Fu:** Writing – review & editing, Methodology, Investigation. **Xiangling Ren:** Writing – review & editing, Methodology, Investigation. **Shiping Yu:** Writing – review & editing, Supervision, Conceptualization. **Xiaowei Chen:** Conceptualization, Writing – original draft, Writing – review & editing. **Nam-Young Kim:** Conceptualization, Writing – review & editing. **Guihua Jiang:** Conceptualization, Writing – review & editing. **Xianwei Meng:** Writing – review & editing, Supervision, Project administration.

Acknowledgments

The authors acknowledge financial support from the Beijing Natural Science Foundation (Nos. 4244112, L248042), the National Natural Science Foundation of China (Nos. 62405333, 62471492, 82172048, U21A20378), the China Postdoctoral Science Foundation (No. 2023M743599), the Postdoctoral Fellowship Program of CPSF (No. GZC20232772), the Science and Technology Cooperation and Exchange Special Project of Shanxi Province (No. 202304041101030), The Science and Education Cultivation Fund of the National Cancer and Regional Medical Center of Shanxi Provincial Cancer Hospital (No. TD2023003), Shanxi Center of Technology Innovation for Controlled and Sustained Release of Nano-drugs (No. 202104010911026).

Supplementary materials

Supplementary material associated with this article can be found, in the online version, at doi:10.1016/j.cclet.2025.111299.

References

[1] R.L. Siegel, K.D. Miller, H.E. Fuchs, A. Jemal, CA Cancer J. Clin. 72 (2022) 7–33.
[2] Y. Qiao, X. Liu, B. Li, et al., Nat. Commun. 11 (2020) 4446.
[3] Q. Du, J. Zou, Z. Huang, et al., Chin. Chem. Lett. 34 (2023) 107763.
[4] Z. Chen, M. Niu, G. Chen, et al., ACS Nano 12 (2018) 12721–12732.
[5] Y. Sun, Z. Chen, H. Gong, et al., Adv. Mater. 32 (2020) e2002024.
[6] Y. Zhu, Z. Yang, Z. Pan, et al., Sci. Adv. 8 (2022) eabo5285.
[7] Y. Zhu, Q. Li, C. Wang, et al., Chem. Rev. 123 (2023) 7326–7378.
[8] X. Ma, Q. Wu, L. Tan, et al., Chin. Chem. Lett. 33 (2022) 1604–1608.
[9] L. Shen, Z. Yang, Y. Zhong, et al., Adv. Sci. 11 (2024) e2406975.
[10] Z. Chen, W. Guo, L. Tan, et al., Adv. Funct. Mater. 34 (2024) 2401359.
[11] W. Zhou, Y. Gao, X. Feng, et al., Chin. Chem. Lett. 36 (2025) 109763.
[12] Z. Xiong, L. Sun, H. Yang, et al., Adv. Funct. Mater. 33 (2022) 2211423.
[13] C. Huang, Z. Liu, L. Zhao, et al., Chin. Chem. Lett. 35 (2024) 109696.
[14] H. Zhu, K. Ma, R. Ruan, et al., Chin. Chem. Lett. 35 (2024) 108536.
[15] Y. Li, S. Xing, F. Chen, et al., Nat. Commun. 14 (2023) 5788.
[16] X. Li, Y. Liu, J. Ke, et al., Adv. Mater. 36 (2024) e2414365.
[17] Y. Chen, J. Zhu, J. Ding, W. Zhou, Chin. Chem. Lett. 35 (2024) 108706.
[18] Y. Guo, Y. Li, M. Zhang, et al., Nat. Commun. 15 (2024) 8586.
[19] G. Hou, Y. Chen, H. Lei, et al., Angew. Chem. Int. Ed. 63 (2024) e202419649.
[20] X. Han, S. Sun, N. Yang, et al., Adv. Funct. Mater. 34 (2024) 2405836.
[21] B. Xu, R. Niu, R. Deng, et al., Adv. Funct. Mater. 34 (2024) 2405265.
[22] L. Chen, X. Ma, W. Liu, et al., Nano Lett. 23 (2023) 8725–8733.
[23] Y. Chen, Y. Lu, H. Lei, et al., ACS Nano 18 (2024) 29913–29929.
[24] S. Liu, Q. Meng, Z. Liu, et al., Angew. Chem. Int. Ed. 63 (2024) e202421402.
[25] T. Chen, K. Liang, J. Wang, et al., Nano Lett. 24 (2024) 14709–14719.
[26] Y. Xu, Y. Wu, X. Zheng, et al., Adv. Sci. 11 (2024) e2411378.
[27] Y. Zhu, X. Wang, L. Feng, et al., Nat. Commun. 15 (2024) 8696.
[28] L. Liu, J. Shi, J. Wang, et al., Adv. Sci. 11 (2024) e2406340.
[29] K.S.G. de Sá, L.A. Amaral, T.S. Rodrigues, et al., Nat. Commun. 14 (2023) 1049.
[30] Z. Zu, J. Sheng, J. Qi, et al., Adv. Funct. Mater. 33 (2023) 2212748.
[31] J. Nie, N. Yang, S. Sun, et al., Angew. Chem. Int. Ed. 63 (2024) e202416426.
[32] Y. Ruan, X. Wu, K. Li, et al., Adv. Funct. Mater. 34 (2024) 2409335.
[33] Y. Chen, C. Wang, Y. Wu, et al., Nat. Nanotechnol. 19 (2024) 1399–1408.
[34] B. Ding, H. Chen, J. Tan, et al., Angew. Chem. Int. Ed. 62 (2023) e202215307.
[35] Y. Zhang, Q. Jia, J. Li, et al., Adv. Mater. 35 (2023) e2305073.
[36] Y. Xiong, C. Xiao, Z. Li, X. Yang, Chem. Soc. Rev. 50 (2021) 6013–6041.